

Multiscale modelling of human gastric electric activity: can the electrogastragram detect functional electrical uncoupling?

M. L. Buist¹, L. K. Cheng², K. M. Sanders³ and A. J. Pullan^{2,4}

¹National University of Singapore, Singapore

²Bioengineering Institute and ⁴Department of Engineering Science, The University of Auckland, New Zealand

³Department of Physiology and Cell Biology, University of Nevada School of Medicine, Reno, NV 89557, USA

During recent years there has been a growing interest in the assessment of gastric electrical health through cutaneous abdominal recordings. The analysis of such recordings is largely limited to an inspection of frequency dynamics, and this has raised doubts as to whether functional gastric electrical uncoupling can be detected using this technique. We describe here a computational approach to the problem in which the equations governing the underlying physics of the problem have been solved over an anatomically detailed human torso geometry. Cellular electrical activity was embedded within a stomach tissue model, and this was coupled to the torso using an equivalent current source approach. Simulations were performed in which normal and functionally uncoupled (through the introduction of an ectopic antral pacemaker) gastric slow wave activity was present, and corresponding cutaneous electrogastragrams were produced. These were subsequently analysed using the currently recommended techniques, and it was found that the functionally uncoupled situation was indistinguishable from normal slow wave activity using this approach.

(Received 30 October 2005; accepted after revision 6 January 2006; first published online 11 January 2006)

Corresponding author M. L. Buist: Division of Bioengineering, National University of Singapore 117576.

Email: biebml@nus.edu.sg

Like the heart, the human stomach generates rhythmic electrical impulses. These electrical impulses (electrical slow waves) control the peristaltic contractions that mix and grind stomach contents (Szurszewski, 1987). Slow waves are initiated by the interstitial cells of Cajal (ICC) in a network that lies in the plane of the myenteric plexus (ICC-MY; see Dickens *et al.* 1999; Ordog *et al.* 1999) and is electrically coupled to the circular and longitudinal muscle layers (Cousins *et al.* 2003). Slow waves actively spread through the ICC and conduct to circular and longitudinal smooth muscle cells. The slow wave depolarization activates voltage-dependent Ca^{2+} channels in smooth muscle cells, and the inward currents activated in smooth muscle cells either sum with currents from ICC-MY to enhance the amplitude and duration of the slow wave or, in some regions, such as the terminal antrum and pylorus, organize into Ca^{2+} action potentials that are superimposed upon the plateau phase of the slow wave. Activation of voltage-dependent Ca^{2+} channels in smooth muscle cells results in Ca^{2+} entry and excitation–

contraction coupling. In the corpus and antral regions of the stomach, the magnitude of peristaltic contractions corresponds to the amplitude and duration of muscle slow waves (Ozaki *et al.* 1991).

In the normal situation, slow waves originate from dominant pacemakers along the greater curvature in the corpus and spread, aborally, through the antrum to the pyloric sphincter. The pacemaker region in the corpus is dominant in the stomach because it generates slow waves at the highest frequency. ICC-MY and pacemaker activity are present in a continuous network from corpus to pylorus, but the pacemaker activity in more distal ICC-MY is slower than in the corpus, allowing the corpus to dominate. In humans, the rate of slow waves in the corpus pacemaker is approximately 3 cycles min^{-1} , and so this is the dominant slow wave frequency in the entire stomach. Disruptions in the network of ICC-MY or breakdown in the frequency gradient along the ICC-MY network from corpus to pylorus can lead to either physical or functional uncoupling of pacemaker activity and block

the proximal to distal spread of gastric peristalsis. This can interrupt normal processing of the gastric contents and delay gastric emptying. Arrhythmias have been associated with a variety of gastric motility disorders, including gastroparesis (Smith *et al.* 2003), gastric myoelectrical dysrhythmia (Qian *et al.* 2003), atrophy and hypertrophy (Bortoff & Sillin, 1986) and diabetic gastropathy (Koch, 2001).

The electrical activity of the stomach can be recorded non-invasively with cutaneous electrodes, giving rise to what is termed the electrogastrogram (EGG). This was first recorded by Alvarez (1922) from 'a little old woman whose abdominal wall was so thin that her gastric peristalsis was easily visible' (Smallwood & Brown, 1983). It was independently discovered again by Davis *et al.* (1957), but it was not until 1975 that the gastric origin of the EGG was conclusively demonstrated (Brown *et al.* 1975). In the last 25 years much has been learnt about the electrical activity of the stomach, and research into the relationship between gastric electrical activity and the EGG has recently increased substantially.

The cutaneous EGG provides an indirect representation of the electrical activity occurring within the abdomen at a small number of recording electrodes. Unlike the standard 12-lead electrocardiogram (ECG) used in electrocardiology, to date no standard has been universally adopted for the number and placement of the EGG electrodes. One system assumes that the lesser curvature of the stomach begins at the xiphoid process and ends at the point where the mid-clavicular line meets the costal margin (Mintchev *et al.* 1993). Using this approach, the most proximal electrode was placed 5 cm to the left of the xiphoid process on the costal margin, and a row of four further electrodes (3 cm apart) were placed linearly between the first electrode and the junction of the mid-clavicular line with the right costal margin. An alternative set-up using two electrodes sites one electrode between the umbilicus and the xyphoid process and the second electrode on the left side of the abdomen, one-third of the distance from the ventral mid-line to the left axial mid-line, 1 cm below the lowest rib (Patterson *et al.* 2001). In yet another approach, Chen *et al.* (1999) used four recording electrodes. The electrodes were centred on a main electrode located 2 cm above the mid-point between the xiphoid process and the umbilicus. Two more electrodes were located on an upper 45 deg angle, with an additional electrode located 4 cm to the right of the central electrode. Arguably the most commonly used set-up in a clinical setting is that described by Koch & Stern (2004) and Jonderko *et al.* (2005). With this system, three electrodes are used to record a single-channel bipolar EGG. A reference electrode was placed on the right side of the abdomen at least 3 cm below the right costal margin. One recording electrode was placed 2–3 cm below the rib cage on the left of the abdomen and the other on the mid-line

equidistant from the xiphoid process and the umbilicus, thus providing a linear arrangement aligned on an axial plane. Owing to its clinical adoption, this electrode set-up will be adopted for our simulations.

Before one can use the EGG to infer the electrical health of the stomach, it is important to understand what is recorded at an EGG electrode, so a brief explanation of this is given here. At the level of a single cell, charged ions move selectively across the outer cell membrane in response to a stimulus (smooth muscle cells) or during pacemaking activity (ICC), changing the potential difference across the cell membrane and generating an active cellular response. At the tissue level, when a cell is activated but its neighbour is not, a potential difference is set up between the adjacent cells. The result of this is a local non-zero current density whose magnitude is determined by the size of the potential difference and the resistivity of the pathway between the cells. To a good approximation, away from this local current density fluctuation the torso acts as a resistive network, allowing the current density profile to be reflected instantaneously as a potential field on the skin surface. Within the torso, the principle of superposition applies, so the electrical potential recorded by an electrode on the skin surface is in fact the sum of all the local cellular current density changes within the stomach. It should be noted that this is not a direct measurement; currents originating from different locations will follow different paths and flow through different tissues on the way to the surface electrode. The contribution of each cell to the final signal is therefore biased by both the distance to the recording site and the resistivity of the current pathway.

In addition to the desired gastric electrical signals, the cutaneous electrodes will record information arising from other sources of electrical activity (e.g. the small intestine, colon and heart, and activity due to respiration and motion). In an attempt to isolate the electrical activity of gastric origin, the frequency components in the recording that are known not to correspond to gastric activity are removed. Removing frequencies below 1 cycle min^{-1} (0.016 Hz) and above 15 cycles min^{-1} (0.25 Hz) has been recommended, thereby creating a bandpass filter (Koch & Stern, 2004). In practice, the signal recorded in the time domain is transformed to the frequency domain through the Fast Fourier Transform (FFT), the unwanted frequency components are removed and the filtered signal is reconstructed via the inverse FFT.

Typically EGG analysis revolves around an investigation of the frequency dynamics of the recordings. In a normal subject, dominant activity at 0.05 Hz (3 cycles min^{-1}) will be observed. With a breakdown in the ICC network, as can occur for instance in diabetes (see Ordog *et al.* 2000), regions of ICC-MY within the gastric network can become uncoupled from the dominant pacemaker, and the synchronized spread of electrical activity from corpus to pylorus is disrupted. In such a situation, ICC-MY

within the antral region may become local pacemakers, and electrical slow waves may be generated in ectopic sites. An increase in the intrinsic frequency of antral pacemakers can lead to functional uncoupling and ectopic pacemaking. This can result in collisions between slow waves propagating from ectopic sites and the normal pacemaker site, disrupting gastric peristalsis and delaying gastric emptying (gastroparesis). A clinical assessment of this condition can lead to various therapeutic techniques to improve gastric emptying and relieve symptoms of gastroparesis. Unfortunately, it may be extremely difficult to evaluate dysrhythmias with a single or even multiple cutaneous sites of recording.

Few modelling studies have been performed with a focus on generating gastric slow waves using anatomically based models. Most mathematical models used to represent the slow wave can be broadly divided into two categories: those that model the stomach as coupled relaxation oscillators and those that attempt to model the underlying physiology. In 1968, Nelsen and Becker suggested that a chain of relaxation oscillators could simulate the electromechanical activity of the small intestine (Nelsen & Becker, 1968). During the early 1970s, Sarna and coworkers further developed this idea, using an array of bi-directionally coupled oscillators to simulate different aspects of gastrointestinal (GI) activity (Sarna *et al.* 1971, 1972). Although these models are capable of recreating the general behaviour of a GI slow wave, the parameters prescribing this behaviour cannot easily be related to the underlying electrical activity occurring at the cellular and tissue level within the walls of the GI tract. Attempts have recently been made to develop models of GI electrical activity at the cellular level with a stronger biophysical base, e.g. Miftakhov *et al.* (1999); Aliev *et al.* (2000). Both of these studies are primarily focused on the small intestine, and at present good cellular models of gastric electrical activity are somewhat lacking.

The geometrical models used in simulations of GI electrical activity within the abdomen have to date been of an idealized nature. These volume conductor models do not include realistic anatomical information and usually model the abdomen as a homogeneous volume conductor (e.g. Bradshaw *et al.* 2003) and the stomach with a simplified conoid or ellipsoid geometry (Mirizzi *et al.* 1986; Mintchev & Bowes, 1998; Irimia & Bradshaw, 2005). In what follows, we describe an anatomically and biophysically based model of the human stomach. This model is used to simulate normal gastric slow waves, and these simulations are shown to be in qualitative agreement with recordings of real slow wave activity. This model is then used to address the issue of functional uncoupling and to examine the issue of whether or not such an event can be detected non-invasively with a commonly used EGG technique.

Methods

An initial model of the human stomach has been created from photographic slices from the Visible Human data set (Spitzer *et al.* 1996). Details of the model development have been described previously by Pullan *et al.* (2003). In brief, the stomach, skin surface and other internal organs were digitized from the axial images. Surface meshes were then created from these data by an iterative linear fitting technique that provided submillimetre accuracy. A volumetric mesh of the stomach wall was subsequently constructed in order to better represent known anatomical features. An illustration of this model is given in Fig. 1A). This process has also been applied to create gastric and torso models from abdominal computed tomography (CT) scans of several patients; an example of this is shown in Fig. 1B).

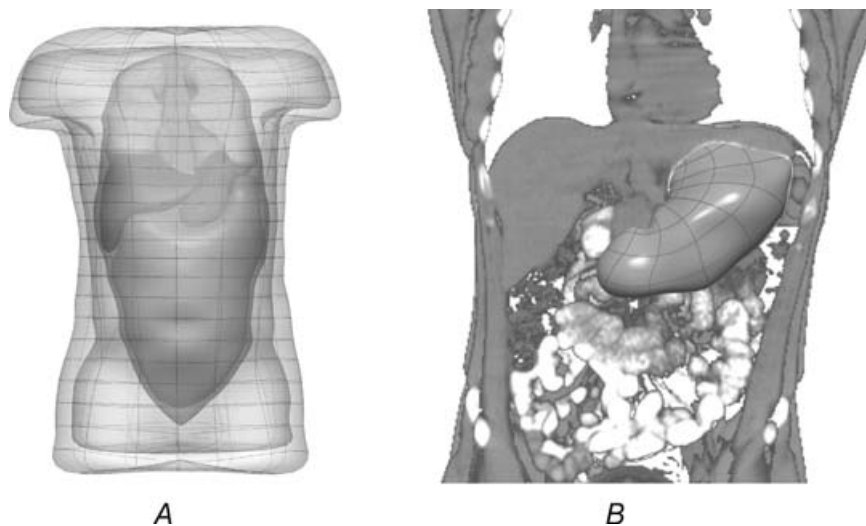


Figure 1. Geometric models of stomach and torso constructed from images from the visible human project (A) and abdominal CT scans (B)

B shows the surface of the stomach model overlaid with a coronal CT image. The subject had ingested oral contrast medium for 1 h prior to imaging. The contrast agent has also progressed through the small intestine.

The muscular architecture within the wall of the stomach that is responsible for the slow wave and subsequent contractions can be described in terms of three muscle layers interspersed with two layers of ICCs (Hirst, 2001). Specifically represented are the outer longitudinal and first circular smooth muscle layers, which are separated by the myenteric layer of ICCs (ICC-MY). Towards the mucosa, a second circular muscle layer is included, which is separated from the first by the septa layer of ICCs (ICC-SEP). This arrangement is illustrated graphically in Fig. 2.

A continuum modelling approach was used to simulate the electrical activity of the stomach. The bidomain model, widely used in simulations of cardiac electrical activity (Plonsey & Barr, 1987; Lines *et al.* 2003), was used to represent the transmembrane and extracellular potentials in the active tissues of the stomach and intestine. These equations are summarized in eqns (1) and (2), where eqn (1) is a reaction–diffusion equation and eqn (2) is a Poisson equation.

$$\begin{aligned} & \nabla \cdot (\sigma_i \nabla V_m) + \nabla \cdot (\sigma_e \nabla \varphi_e) \\ & = A_m \left(C_m \left\{ \frac{\partial V_m}{\partial t} \right\} + I_{\text{ion}} \right) \end{aligned} \quad (1)$$

$$\nabla \cdot (\{\sigma_i + \sigma_e\} \nabla \varphi_e) = -\nabla \cdot (\sigma_i \nabla V_m) \quad (2)$$

The subscripts *i* and *e* represent properties of the intracellular and extracellular domains, respectively. The σ terms are tissue conductivities (which in general will be tensors), the φ terms are potentials, V_m is the transmembrane potential (the potential difference across the cell membrane), A_m is the surface-to-volume ratio of the continuum cell membrane, and C_m is the membrane capacitance. It should be noted that after Aliev *et al.* (2000), the intracellular current flow between the smooth muscle and ICC layers was modelled using a linear potential difference, as opposed to the diffusive coupling specified by the bidomain equations and employed in the remainder of the stomach. The contributions of the local ionic currents from single cells interact with the continuum through the I_{ion} term in the eqn (1). This allows complex cellular dynamics to be incorporated without a consequential increase in the complexity of the tissue level model.

The large derivative continuous elements that describe the stomach geometry as illustrated in Fig. 1B are insufficient for capturing the gastric slow wave. Therefore each of these volume elements is divided into a large number of smaller hexahedra within the local normalized space of each geometric element. The result is a high-resolution structured hexahedral mesh over which the bidomain equations can be successfully solved using the finite element method.

At each vertex in the high-resolution stomach mesh, a description of cellular electrical activity is placed. A modified FitzHugh–Nagumo (FHN) model (FitzHugh, 1961; Nagumo *et al.* 1962; Aliev *et al.* 2000) was used to model the electrical activity of the muscle cells and ICCs, since this currently appears to be the most advanced model that explicitly differentiates between the different cell types (ICCs and smooth muscle). The cellular equations are based on a normalized transmembrane potential, u , that varies from 0 to 1, and a single recovery variable, v . These equations are:

$$\frac{du}{dt} = ku(u - a)(1 - u) - v \quad (3)$$

$$\frac{dv}{dt} = \varepsilon(\gamma \{u - \beta\} - v) \quad (4)$$

where k is the maximum membrane conductance, a is the normalized threshold potential, ε controls the excitability of the system, γ is the recovery rate constant and β is used to shift the cellular equilibrium from an excitatory to an oscillatory state. The values of the parameters described in the original paper of Aliev *et al.* (2000) have been modified to match published serosal recordings of gastric slow wave (Bauer *et al.* 1985), and a full description of these parameter values may be found in Buist *et al.* (2004).

The above equations are sufficient to simulate a gastric slow wave. However, to calculate the corresponding potentials on the torso surface that arise from this slow wave, two further steps were employed. First, the local current density changes prescribed by the (continuum) cellular electrical activity were expressed as equivalent dipole sources. These dipole sources were then used to compute the electrical potential field on the surface of the torso volume conductor. The equivalent dipole sources (\mathbf{J})

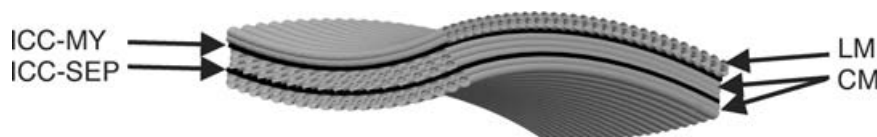


Figure 2. A cross-section of the musculature within a small section of the stomach wall

This consists of a longitudinal muscle layer (LM) and two circular muscle layers (CM). The LM and outer CM layer are separated by ICCs from the myenteric plexus (ICC-MY), and the circular muscle layers are separated by the ICC septa layer (ICC-SEP). The serosa is found closest to the LM layer and the mucosa is closest to the CM layer.

are computed from the transmembrane potential gradient as shown in eqn (5).

$$\mathbf{J} = - \left(\left\{ \frac{\sigma_i \sigma_e}{\sigma_i + \sigma_e} \right\} \nabla V_m \right) \quad (5)$$

Here σ_i and σ_e are the intra- and extracellular conductivities and V_m is the transmembrane potential. Each dipole source has a centre and orientation that varies over time to describe the location, direction and strength of the local electrical activity. These dipole sources are then used to compute the electrical fields within the torso surface by solving the Poisson equation:

$$\nabla (\sigma_e \nabla \phi) = \nabla \cdot \mathbf{J} \quad (6)$$

where the source term \mathbf{J} is due to the equivalent dipole sources and is the torso potential field.

A typical solution then consists of three sets of calculations that must be performed at each time step. First the cellular models are updated throughout the active stomach. Next the transmembrane and extracellular potentials are calculated from the cellular activity and known diffusive tissue properties. The equivalent gastric dipolar sources are then created and the passive torso volume conductor problem is then solved to calculate the electric field throughout the torso. Using this equation set, the resulting electrical activity at electrodes on the body surface can be determined from the (continuum) cellular level activity. The numerical accuracy of this modelling framework has been demonstrated previously in a number of tests (Pullan *et al.* 2003).

Results

Two sets of simulations were run to test the hypothesis that the EGG recording and interpretation system described earlier is unable to differentiate between normal and abnormal slow wave patterns when an ectopic antral pacemaker is present. Owing to the presence of spontaneously active ICCs in the model, no external stimulus was required to initiate or maintain slow waves. Within the ICC model of Aliev *et al.* (2000), the excitability parameter is the main determinant of pacemaker frequency, so by incorporating this as a spatially varying parameter the desired initial activation sites can be specified. Under normal conditions the ICC excitability was at a maximum in the proximal corpus on the greater curvature, decreasing slightly circumferentially and more prominently longitudinally (see Buist *et al.* 2004 for details). To describe the ectopic antral pacemaker, the ICC excitability in the terminal antrum was adjusted to mirror that of the primary pacemaker site in the proximal corpus. Conduction velocities within the stomach were matched to the experimental data from Familoni *et al.* (1987).

The membrane potential at rest and at the peak of the slow wave was set in accordance with the experimental data from Horiguchi *et al.* (2001) and Bauer *et al.* (1985). These studies demonstrated that the resting membrane potential is lower in the regions with dense ICC networks. In the smooth muscle layers, the resting membrane potential was set to -60 mV with a peak potential of -38 mV, and in the ICC layers the resting potential was set to -73 mV with a peak potential of -32 mV, thus providing a degree of electrotonic coupling even under resting conditions.

The stomach volume and torso surface geometries derived from the visible human data set (shown in Fig. 1A) were used for these simulations. In order to solve the bidomain equations accurately over the electrically active stomach, a high-resolution structured finite element mesh was embedded within the volume elements of the stomach wall at an average spatial resolution of less than 1 mm. For both the normal and abnormal situations, 300 s of gastric electrical activity was simulated using a time step of 50 ms, giving a total of 6000 time steps. At every time step, one dipole source was calculated within each of the 320 elements used to describe the stomach geometry, meaning that each source represented the net electrical activity from an element. The resulting 320 dipole sources were placed within the boundary element torso surface model (comprising 300 derivative continuous surface elements), and eqn (6) was solved to generate the body surface potential distribution. From these data, monopolar EGG traces were extracted, providing a simulated sampling frequency of 20 Hz. An example of the results obtained from these simulations is shown in Fig. 3, where the results in the upper panel arise from normal slow wave activity and the results in the lower panel show equivalent results when an ectopic antral pacemaker is present.

In both cases, the geometry and location of the stomach were unchanged and therefore, as expected, the bulk of the electrical activity can be seen on the abdomen over the stomach. Although sizeable differences can be observed at some time points, at others the difference in the potential field would be difficult to categorize. In the left panel of Fig. 3B, it can be clearly seen that the slow waves from the normal and ectopic pacing sites will collide (and be extinguished), preventing the slow wave initiated in the proximal corpus from reaching the pylorus and resulting in functional gastric uncoupling.

The potential field was recorded at each solution time point from the three locations indicated on the torso surface in Fig. 3. From these data, a single bipolar trace was constructed for the normal and abnormal situations, as is done in the experimental EGG recording procedure. The resulting bipolar EGG traces are displayed in Fig. 4A and B.

An inspection of the EGG traces shows some shape and amplitude variations. However, it is unlikely that either of these measures would provide enough information to

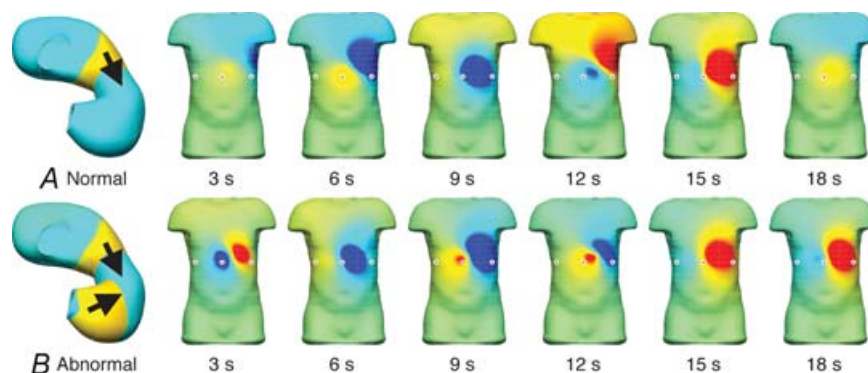


Figure 3. Simulated body surface EGGs

The left panel of *A* shows a normal gastric slow wave generated in the proximal corpus. The arrow indicates the aboral direction of propagation. The remaining panels in *A* show the body surface potential distribution at six time points during a single slow wave cycle. The three indicated positions on the front of the torso indicate the location of the simulated EGG electrodes. The left panel of *B* shows a normal gastric slow wave and a second slow wave from the antral pacemaker that is moving in an oral direction. The remaining panels in *B* show the body surface potential distribution at six time points corresponding to this abnormal activation sequence. In the stomach images, light blue tissue is quiescent and yellow/red tissue is activated. The oesophageal junction is located at the upper opening and the pyloric sphincter at the lower opening. In the torso images, blue represents negative potentials and red represents positive potentials relative to a zero reference on the right hip.

make a diagnosis, since both of these parameters will vary with the shape and body composition of the subject and variations in electrode placement. EGG amplitude is also affected experimentally by the quality of the contact between the electrodes and the skin surface. Experimentally recorded EGG traces using this set-up can be found in Koch & Stern (2004), and with an alternative electrode configuration in Chen *et al.* (1999). As is currently standard procedure, the power spectrum

of the two signals was computed, and these results are shown in Fig. 4*C* and *D*. In both cases, there is clearly a dominant pacemaking frequency at close to 0.055 Hz or 3.3 cycles min^{-1} (0.055 and 0.056 Hz for the normal and abnormal cases, respectively). This agrees with the dominant frequency observed experimentally in normal human subjects (Bradshaw *et al.* 1999). The normal case shows a clear second harmonic; such harmonics are commonly found in experimental recordings and

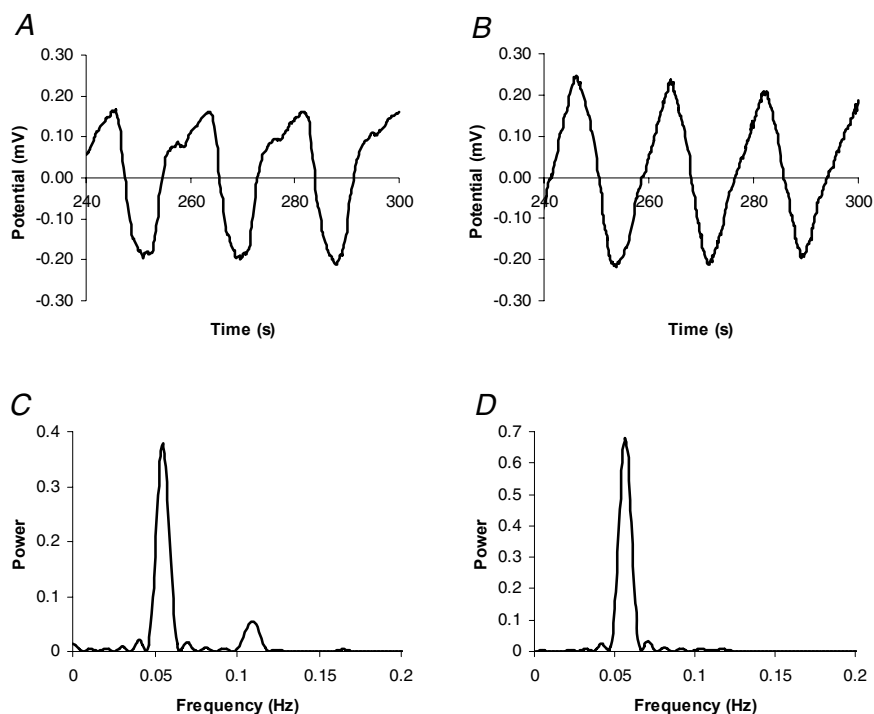


Figure 4

A and *B* show single channel bipolar electrogastragrams recorded from the epigastric surface of the model. *A* was generated from pacemaker activity in the proximal corpus at 3 cycles min^{-1} (0.05 Hz). *B* was generated using the same pacemaker activity as *A*, with the addition of a secondary pacemaker in the gastric antrum, also at 3 cycles min^{-1} . *C* and *D* show the power spectra for the normal case and the case with the secondary antral pacemaker, respectively.

therefore cannot be used to distinguish between the two cases. Interestingly, the abnormal simulation with the secondary antral pacemaker generated slightly larger EGG signals. As mentioned previously, the EGG represents the net underlying activity and therefore it is likely that there is more reinforcement and/or less cancellation of the cellular-based current sources in this situation.

Discussion

The integrated electrical activity of the phasic regions of the stomach (i.e. sites distal to the orad corpus) depends upon the frequency gradient that is intrinsic to ICC-MY in the proximal and distal stomach (see Ordog *et al.* 2002). Enhancement in antral frequency or retardation in corpus frequency can lead to a situation in which there is not time for corpus slow waves to propagate to the pylorus before discharge of a distal pacemaker. Breakdown in the proximal-to-distal pacemaker frequency can lead to functional uncoupling of slow wave propagation, disruption of gastric peristalsis and delayed gastric emptying. Functional uncoupling could occur, for example, if the intrinsic frequency of antral pacemakers approaches the frequency of the dominant corpus pacemaker (i.e. antral pacemaker increases to 2–3 cycles min^{-1}). Thus, it is important for clinicians to be able to properly evaluate more than gastric electrical frequency; they must be able to assess the spread of gastric slow waves from the corpus to the antrum (functional coupling).

In this study we have described our computational model of the gastric slow wave and the resulting abdominal EGG recordings. Both normal and abnormal slow wave activity have been simulated, and bipolar EGG traces have been generated to mimic what is recorded in the clinical situation. An analysis of the frequency dynamics of these EGG traces, as is standard practice with such recordings, has revealed that this metric was not able to distinguish between normal gastric slow wave activity and functional gastric uncoupling caused by a secondary antral pacemaker. Although this computational evidence is presented here for only a single pacing abnormality, we believe that in fact a wide range of conditions exhibiting functional uncoupling would be undetectable using the EGG technique selected for this study. For example, if the primary pacemaker in the proximal corpus was damaged, an antral pacemaker could produce retrograde slow waves that transverse the length of the active stomach. This would produce a single dominant frequency and return a normal diagnosis if the pacing was within the range of frequencies considered clinically normal (between 2.5 and 3.75 cycles min^{-1} ; Koch & Stern, 2004). The simulations performed here demonstrate that in fact it is not even necessary for the primary pacing site to be disrupted in order to get EGG traces with a

single dominant frequency within the normal range but functional electrical uncoupling.

In the cardiac arena, the sensitivity of ECG recordings to geometric factors has been well documented, along with a relative insensitivity to the composition of the passive torso volume (Bradley *et al.* 2000). At present these remain open questions in relation to the EGG. We are currently moving to address these issues and have begun the task of constructing patient-specific stomach and torso models from medical images for this purpose.

From a clinical perspective, it is very important to determine whether slow waves in the corpus propagate in a normal manner and drive the pacemaker activity of the distal stomach. This requires high-fidelity recording of electrical activity from more than a single site, placement of electrodes in a serial manner from corpus to distal antrum, and a means to analyse records for aberrant propagation. It may be that these requirements exceed the capacity of cutaneous recordings of gastric electrical activity. Focal changes in intrinsic pacemaker frequency of the order that can lead to functional uncoupling would be extremely difficult to discern with present EGG techniques, and the EGG does not appear to be reliable enough to accomplish evaluation of directional propagation. Gastric serosal surface recording, which would provide the most reliable means of evaluation, is not practical because of its invasive nature. We would suggest that multipoint luminal recording, after placement of electrodes via endoscope, might provide the most suitable means of reliable clinical recording of gastric electrical activity. This technique is now being tried in some clinical gastroenterology units.

References

- Aliev RR, Richards WO & Wikswo JP (2000). A simple nonlinear model of electrical activity in the intestine. *J Theor Biol* **204**, 21–28.
- Alvarez WC (1922). The electrogastrogram and what it shows. *J Am Med Assoc* **78**, 1116–1119.
- Bauer AJ, Publicover NG & Sanders KM (1985). Origin and spread of slow waves in canine gastric antral circular muscle. *Am J Physiol* **249**, G800–G806.
- Bortoff A & Sillin LF (1986). Changes in intercellular electrical coupling of smooth muscle accompanying atrophy and hypertrophy. *Am J Physiol* **250**, C292–C298.
- Bradley CP, Pullan AJ & Hunter PJ (2000). Effects of material properties and geometry on electrocardiographic forward simulations. *Ann Biomed Eng* **28**, 721–741.
- Bradshaw LA, Ladipo JK, Staton DJ, Wikswo JP Jr & Richards WO (1999). The human vector magnetogastrogram and magnetoenterogram. *IEEE Trans Biomed Eng* **46**, 959–970.
- Bradshaw LA, Myers A, Wikswo JP & Richards WO (2003). A spatio-temporal dipole simulation of gastrointestinal magnetic fields. *IEEE Trans Biomed Eng* **50**, 836–847.
- Brown BH, Smallwood RH, Duthie HL & Stoddard CJ (1975). Intestinal smooth muscle electrical potentials recorded from surface electrodes. *Med Biol Eng* **13**, 97–103.

- Buist ML, Cheng LK, Yassi R, Bradshaw LA, Richards WO & Pullan AJ (2004). An anatomical model of the gastrointestinal system for producing bioelectric and biomagnetic fields. *Physiol Meas* **25**, 849–861.
- Chen JD, Zou X, Lin X, Ouyang S & Liang J (1999). Detection of gastric slow wave propagation from the cutaneous electrogastrogram. *Am J Physiol* **277**, G424–G430.
- Cousins HM, Edwards FR, Hickey H, Hill CE & Hirst GD (2003). Electrical coupling between the myenteric interstitial cells of Cajal and adjacent muscle layers in the guinea-pig gastric antrum. *J Physiol* **550**, 829–844.
- Davis RC, Garafolo L & Gault FP (1957). An exploration of abdominal potential. *J Comp Physiol Psychol* **52**, 519–523.
- Dickens EJ, Hirst GD & Tomita T (1999). Identification of rhythmically active cells in guinea-pig stomach. *J Physiol* **514**, 515–531.
- Familoni BO, Kingma YJ & Bowes KL (1987). Study of transcutaneous and intraluminal measurement of gastric electrical activity in humans. *Med Biol Eng Comput* **25**, 397–402.
- FitzHugh RA (1961). Impulses and physiological states in theoretical models of nerve membrane. *Biophys. J.* **1**, 445–466.
- Hirst GDS (2001). An additional role for ICC in the control of gastrointestinal motility? *J Physiol* **537**, 1.
- Horiguchi K, Semple GS, Sanders KM & Ward SM (2001). Distribution of pacemaker function through the tunica muscularis of the canine gastric antrum. *J Physiol* **537**, 237–250.
- Irimia A & Bradshaw LA (2005). Ellipsoidal electrogastrographic forward modelling. *Phys Med Biol* **50**, 4429–4444.
- Jonderko K, Kasicka-Jonderko A & Blonska-Fajfrowska B (2005). Does body posture affect the parameters of a cutaneous electrogastrogram? *J Smooth Muscle Res* **41**, 133–140.
- Koch KL (2001). Electrogastrography: physiological basis and clinical application in diabetic gastropathy. *Diabetes Tech Therap* **3**, 51–62.
- Koch KL & Stern RM (2004). *Handbook of Electrogastrography*. Oxford University Press, New York.
- Lines GT, Buist ML, Grottum P, Pullan AJ & Tveito A (2003). Mathematical models and numerical methods for the forward problem in cardiac electrophysiology. *Comput Vis Sci* **5**, 215–239.
- Miftakhov RN, Abdusheva GR & Christensen J (1999). Numerical simulation of motility patterns of the small bowel. 1. Formulation of a mathematical model. *J Theor Biol* **197**, 89–112.
- Mintchev MP & Bowes KL (1998). Computer simulation of the effect of changing abdominal thickness on the electrogastrogram. *Med Eng Phys* **20**, 177–181.
- Mintchev MP, Bowes KL & Kingma YJ (1993). Accuracy of cutaneous recordings of gastric electrical activity. *Gastroenterology* **104**, 1273–1280.
- Mirizzi N, Stella R & Scafoglieri U (1986). Model to simulate the gastric electrical control and response activity on the stomach wall and on the abdominal surface. *Med Biol Eng Comput* **24**, 157–163.
- Nagumo J, Animoto S & Yoshizawa S (1962). An active pulse transmission line simulating nerve axon. *Proc Inst Radio Engineers* **50**, 2061–2070.
- Nelsen TS & Becker JC (1968). Simulation of the electrical and mechanical gradient of the small intestine. *Am J Physiol* **214**, 749–757.
- Ordog T, Baldo M, Danko R & Sanders KM (2002). Plasticity of electrical pacemaking by interstitial cells of Cajal and gastric dysrhythmias in W/W mutant mice. *Gastroenterology* **123**, 2028–2040.
- Ordog T, Takayama I, Cheung WK, Ward SM & Sanders KM (2000). Remodeling of networks of interstitial cells of Cajal in a murine model of diabetic gastroparesis. *Diabetes* **49**, 1731–1739.
- Ordog T, Ward SM & Sanders KM (1999). Interstitial cells of cajal generate electrical slow waves in the murine stomach. *J Physiol* **518**, 257–269.
- Ozaki H, Stevens RJ, Blondfield DP, Publicover NG & Sanders KM (1991). Simultaneous measurement of membrane potential, cytosolic Ca²⁺, and tension in intact smooth muscles. *Am J Physiol* **260**, C917–C925.
- Patterson M, Rintala TR, Lloyd TD, Abernethy L, Houghton TD & Williams J (2001). Validation of electrode placement in neonatal electrogastrography. *Dig Dis Sci* **46**, 2245–2249.
- Plonsey R & Barr RC (1987). Mathematical modelling of electrical activity of the heart. *J Electrocardiol* **20**, 219–226.
- Pullan AJ, Cheng LK, Yassi R & Buist ML (2003). Modelling gastrointestinal bioelectric activity. *Prog Biophys Mol Biol* **85**, 523–550.
- Qian LW, Pasricha PJ & Chen JDZ (2003). Origins and patterns of spontaneous and drug-induced canine gastric myoelectrical dysrhythmia. *Digest Dis Sci* **48**, 508–515.
- Sarna SK, Daniel EE & Kingma YJ (1971). Simulation of slow-wave electrical activity of small intestine. *Am J Physiol* **221**, 166–175.
- Sarna SK, Daniel EE & Kingma YJ (1972). Premature control potentials in the dog stomach and in the gastric computer model. *Am J Physiol* **222**, 1518–1523.
- Smallwood RH & Brown BH (1983). Non-invasive assessment of gastric activity. In *Non-invasive Physiological Measurements*, vol. 2, ed. Rolfe P, pp. 179–217. Academic Press, London.
- Smith DS, Williams CS & Ferris CD (2003). Diagnosis and treatment of chronic gastroparesis and chronic intestinal pseudo-obstruction. *Gastroenterol Clin North Am* **32**, 619–658.
- Spitzer V, Ackerman MJ, Scherzinger AL & Whitlock D (1996). The visible human male: a technical report. *J Am Med Inform Assoc* **3**, 118–130.
- Szurszewski JH (1987). Electrical basis for gastrointestinal motility. In *Physiology of the Gastrointestinal Tract*, ed. Johnson LR, pp. 383–422. Raven, New York.